Central neurogenetic signatures of the visuomotor integration system

Elisenda Bueichekú[a,b], Maite Aznárez-Sanado[c,d], Ibai Diez[a,e], Federico d'Oleire Uquillas[f,g], Laura Ortiz-Terán[a,h], Abid Y. Qureshi[i,j], Maria Suñol[a,k,l,m], Silvia Basaia[a,n], Elena Ortiz-Terán[a], Maria A. Pastor[c], and Jorge Sepulcre[a,i,1]

[a]Gordon Center for Medical Imaging, Department of Radiology, Massachusetts General Hospital, Harvard Medical School, Boston, MA 02115; [b]Department of Basic Psychology, Clinical Psychology and Psychobiology, Jaume I University, 12071 Castelló de la Plana, Spain; [c]Neuroimaging Laboratory, School of Medicine, University of Navarra, 31008 Pamplona, Spain; [d]School of Education and Psychology, University of Navarra, 31008 Pamplona, Spain; [e]Neurotechnology Laboratory, Health Department, Tecnalia, E-48160 Derio, Spain; [f]Princeton Neuroscience Institute, Princeton University, Princeton, NJ, 08540; [g]Department of Neurology, Massachusetts General Hospital, Harvard Medical School, Charlestown, MA 02129; [h]Department of Radiology, Brigham and Women's Hospital, Boston MA 02115; [i]Athinoula A. Martinos Center for Biomedical Imaging, Department of Radiology, Massachusetts General Hospital, Harvard Medical School, Charlestown, MA 02129; [j]Department of Neurology, University of Kansas Medical Center, Kansas City, MO 66160; [k]Psychiatry Department, Bellvitge University Hospital, Institut d'Investigació Biomèdica de Bellvitge (IDIBELL), 08907 L'Hospitalet de Llobregat, Barcelona, Spain; [l]Center for Biomedical Research in Mental Health Network, Carlos III Health Institute, 08907 L'Hospitalet de Llobregat, Barcelona, Spain; [m]Department of Clinical Sciences, School of Medicine, University of Barcelona, 08036 Barcelona, Spain; and [n]Neuroimaging Research Unit, San Raffaele Scientific Institute, Vita-Salute San Raffaele University, 20132 Milan, Italy

Edited by Marcus E. Raichle, Washington University in St. Louis, St. Louis, MO, and approved February 5, 2020 (received for review July 18, 2019)

Visuomotor impairments characterize numerous neurological disorders and neurogenetic syndromes, such as autism spectrum disorder (ASD) and Dravet, Fragile X, Prader–Willi, Turner, and Williams syndromes. Despite recent advances in systems neuroscience, the biological basis underlying visuomotor functional impairments associated with these clinical conditions is poorly understood. In this study, we used neuroimaging connectomic approaches to map the visuomotor integration (VMI) system in the human brain and investigated the topology approximation of the VMI network to the Allen Human Brain Atlas, a whole-brain transcriptome-wide atlas of cortical genetic expression. We found the genetic expression of four genes—TBR1, SCN1A, MAGEL2, and CACNB4—to be prominently associated with visuomotor integrators in the human cortex. TBR1 gene transcripts, an ASD gene whose expression is related to neural development of the cortex and the hippocampus, showed a central spatial allocation within the VMI system. Our findings delineate gene expression traits underlying the VMI system in the human cortex, where specific genes, such as TBR1, are likely to play a central role in its neuronal organization, as well as on specific phenotypes of neurogenetic syndromes.

visuomotor integration | TBR1 | brain functional networks | functional connectivity | genetics

Convergence of visual and motor neural circuits is fundamental for successful adaptation in humans. On a moment-to-moment basis, appropriate adjustment to a changing environment relies on a perception–action cycle, that is, the ability to process sensorial inputs and produce coherent motor responses. Not surprisingly, altered visuomotor integration (VMI) has a profound functional impact on daily-life motoric behaviors. A wide variety of neurological disorders and neurogenetic syndromes have been associated with VMI dysfunction within the perception–action cycle. For example, syndromes such as Dravet (1–3), Fragile X (4), Prader–Willi (5–7), Turner (8–10), and Williams syndromes (11, 12) and Autism Spectrum Disorder (ASD) (13, 14) are characterized by compromised VMI in terms of the ability to interactively coordinate visual perception and fine motor skills (15, 16). Although a great variety of genes have been proposed as a possible etiology for these syndromes (*SI Appendix*, Table S1), some present phenotypic overlap and comorbidity between them (e.g., ASD and Fragile X, Prader–Willi, and Turner) (17–19). This underappreciated pattern suggests the possibility that specific genetic backgrounds and interactions between genes could have direct effects on VMI-related circuits, in turn manifesting as atypical cognitive–behavioral adaptations to the changing environment.

To date, it remains unknown what genetic traits support the human VMI system. Following well-known clinical characterizations of the aforementioned neurogenetic syndromes (ASD, Dravet, Fragile X, Prader–Willi, Turner, and Williams syndromes), we hypothesized that the VMI network must overlap with specific patterns of gene expression along the brain's functional architecture, setting a substratum for typical and atypical VMI functioning. In this study we aimed to first describe the cortical functional network that supports the VMI system using a graph theory analysis based on functional connectivity MRI both at rest and task. Briefly, cohort 1 participants completed a finger-tapping task during MRI scanning (see *Methods* and *SI Appendix* for more detailed information). The task consisted of learning and reproducing sequences of finger movements, thus integrating visual information and motor performance. Colored circles, which assigned a color to each finger, were used to present the sequence of finger movements (color 1: little finger, color 2: ring finger, color 3: middle finger, color 4: index finger). The only data used in our analysis were those which related to the ordered sequence of movements (e.g., 1–2–3–4–1–2–3–4) and the bimanual performance. Second, we used the Allen Human Brain Atlas (AHBA) (20) and genetic

Significance

Previous research has explored the association between behavioral disorders and dysfunction in corresponding neural networks. For example, autism spectrum disorder, Prader–Willi syndrome, and Dravet syndrome are characterized by behavioral deficits in the visuomotor integration system. To date, few investigations have combined brain connectomic–genetic data to investigate the biological basis of childhood neurodevelopment and clinical syndromes. The present study provides evidence of a link between expression of malfunctioning genes associated with these syndromes (i.e., TBR1, SCN1A, MAGEL2, and CACNB4) and cortical distribution across regions devoted to integrating visual and motor information (i.e., the lateral occipital cortex, OP4, and intraparietal sulcus). We suggest this altered gene expression may underlie brain network dysfunction which, in turn, leads to behavioral deficits.

Author contributions: E.B., M.A.-S., I.D., S.B., M.A.P., and J.S. designed research; E.B., M.A.-S., I.D., F.d.U., L.O.-T., A.Y.Q., M.S., E.O.-T., and J.S. performed research; E.B., I.D., S.B., and J.S. analyzed data; and E.B., M.A.-S., I.D., F.d.U., L.O.-T., M.S., S.B., E.O.-T., M.A.P., and J.S. wrote the paper.

The authors declare no competing interest.

This article is a PNAS Direct Submission.

[1]To whom correspondence may be addressed. Email: sepulcre@nmr.mgh.harvard.edu.

This article contains supporting information online at https://www.pnas.org/lookup/suppl/doi:10.1073/pnas.1912429117/-/DCSupplemental.

First published March 6, 2020.

enrichment analyses (21) to examine genetic expression patterns delineated by the cortical map related to the VMI system. Third, we investigated the association between gene expression patterns of the VMI network and genes previously associated with neurogenetic syndromes characterized by VMI impairments. In summary, we used a large-scale neuroimaging–connectomic–genetic strategy to unveil the brain connectivity supporting the VMI system and then uncovered the protein-coding genes whose gene expression profiles were most related to this system.

Results

VMI Maps. After performing a whole-brain voxel-level analysis of the VMI task, we found significant activation in lateral inferior and middle occipital cortex (BA 19, 37), sensorimotor cortex (BA 2, 3, 4, 6), posterior middle temporal gyrus (BA 20, 21, 37), parietal opercula (OP1 to OP4), angular and supramarginal parietal cortices (BA 39, 40), supplementary motor area and dorsal anterior cingulate cortex (BA 24, 32), bilateral cerebellum (area 6, area 8, vermis 6, 7, and 8), and bilateral posterior fusiform gyri (BA 19) (cohort 1, significance corrected threshold at $q < 0.001$ false discovery rate [FDR]; Fig. 1*A*).

Next, we calculated the brain areas that interconnect V1 and M1 using stepwise functional connectivity (SFC), that is, areas that accumulate a high significant number of connections toward both V1 and M1 concurrently (significance corrected threshold at $q < 0.001$ FDR; Fig. 1*A*). This whole-brain voxel-level analysis was performed independently in task MRI data (cohort 1) and resting-state MRI data (cohort 2). We found that specific regions of the cerebral cortex display visuomotor interconnector properties, namely, the medial and lateral inferior occipital gyri (BA 17, 18, and 19), middle occipitotemporal cortex (BA 37), sensorimotor cortex (BA 2, 3, 4, and 6), bilateral posterior fusiform gyrus (BA 19), precuneus and posterior cingulate gyrus, parietal opercula (OP1 to OP4), angular and supramarginal parietal cortices (BA 39 and 40), supplementary motor area and dorsal anterior cingulate cortex (BA 24 and 32), and anterior insula/inferior frontal cortex (BA 47, 48, 44, and 45).

Finally, we obtained a consensus VMI map by averaging the normalized multimodal images, that is, the task activation, task connectivity, and resting-state connectivity maps, which highlighted the common brain areas involved in the performance of our VMI task and the interconnectivity between V1 and M1 (Fig. 1*B*). Medial occipital regions, specific areas of the motor cortex (BA 4 to BA 6), regions of the posterior to anterior cingulate gyrus including part of the precuneus and perisylvian areas (OP1 to OP4), and posterior to anterior insula and ventrolateral inferior frontal gyrus were all found to be related to the integration of the visual and motor systems.

Genes with Cortical Expression within the VMI System. The VMI map displayed a high spatial similarity with 485 genes along the entire cerebral transcriptome of 20,737 genes from the AHBA. A Gene Ontology (GO) Protein Analysis Through Evolutionary Relationships (PANTHER) overrepresentation analysis of these 485 genes identified significant roles in specific biological processes and cellular components annotations (binomial test; significance corrected threshold at $q < 0.05$ FDR and fold enrichment [FE] >2). Particularly, we found that cell communication by electrical coupling, as well as different domains of the cellular transmembrane transport drove the main biological processes of the reported genes (Fig. 1*C*). This set of genes displayed an overrepresentation of specific cellular components circumscribed to insulin receptor complex (FE = 26.75), Na/P exchanging ATPase (FE = 14.86), cation channel complex (FE = 2.97), as well as key parts of neurons such as neuronal cell body membrane (FE = 8.26), axon (FE = 2.03), and GABA-ergic synapse (FE = 4.57). Moreover, we discovered that the cortical expression of four a priori genes selected from neurogenetic syndromes with VMI alterations—*TBR1* ($r = 0.606$; Fig. 1*D*), *SCN1A* ($r = 0.526$), *MAGEL2* ($r = 0.499$), and *CACNB4* ($r = 0.489$) (see *SI Appendix*, Fig. S1)—had high spatial similarity with the VMI map (Fig. 1*C*; significance corrected threshold at $q < 0.001$ FDR). An interactome-based validation approach with independent gene–gene interaction profiles demonstrated that TBR1, and to a lesser extent CACNB4 and MAGEL2, was centrally localized in its position within the genetic interaction network of the VMI-related genes (Fig. 2 *A* and *B*). Results of another validation approach are presented in *SI Appendix*, Fig. S2. A visualization of the cortical distribution of the transcripts of TBR1, SCN1A, MAGEL2, and CACNB4 appears in *SI Appendix*, Fig. S3.

Discussion

Successful performance of a variety of common daily tasks relies on the smooth interaction between visual processing and motor responses. Different neuroclinical phenotypes and neurogenetic syndromes have been related to behavioral deficits in the VMI system [e.g., ASD (22), Dravet syndrome (3, 23), and Prader–Willi syndrome (6)] or processes closely related to VMI, such as visual perception and fine motor coordination, or other cortical processes like motor inhibition and sustained attention (24). In this study, we aimed to close the gap in the understanding of the biological process behind perception-to-action in humans and characterize the genetic basis underlying the integration of visual and motor functions. By doing so, we have delineated the cortical genetic background associated with VMI, where specific genes, such as *TBR1*, are likely to play a central role in its neuronal organization.

VMI Network: Anatomical and Connectomic Theories. During the last few decades there has been a growing interest in studying and characterizing how the brain links perception to action (25). While segregation approaches, in which sensory and motor systems are studied in isolation, have been beneficial for understanding the numerous mechanisms that mediate functions of modal systems, there is a need for approaches that assess their direct integration in order to better understand brain system function, particularly in syndromes characterized by compromised goal-directed behavior. This is one of the main contributions of the present research: a connectomic approach was used to link brain activity during performance of a VMI task with brain anatomy and connectivity at rest. The finger-tapping task was used as an easy-to-implement task to study how the brain processes visual information and produces coherent motor responses according to task goals. The brain network supporting the finger-tapping task highly overlapped with resting-state functional connectivity of the primary visual cortex and the primary motor area. A final consensus map allowed us to describe a fine-tuned map of the VMI regions in the human brain. This emphasized the role of the lateral occipital, intraparietal sulcus (IPS) and perisylvian regions in the OP and frontal operculum areas as the main regions supporting the topology of the VMI network. Activity in the lateral occipital cortex has been associated with specific object representations in the visual cortex (26). This area responds to both visual and haptic object recognition, and the response is greater when the object is presented in these modalities at the same time (27–29). OP4 has been identified as a key region for sensorimotor integration (30, 31). Its activity has been associated with hand visuomotor stimulation (32, 33), finger object manipulation, and discrimination and recognition (34, 35), as well as motor learning and visual perceptual-related functions after motor learning (36, 37). The IPS is a well-described attention area that supports the integration of visual inputs and cognitive information by using priority maps (e.g., refs. 38–43). At the functional level, the IPS has been related to VMI in studies involving static (44) and moving objects (45).

Neuroimaging evidence found in the present research is well aligned with cognitive theories related with visual processing,

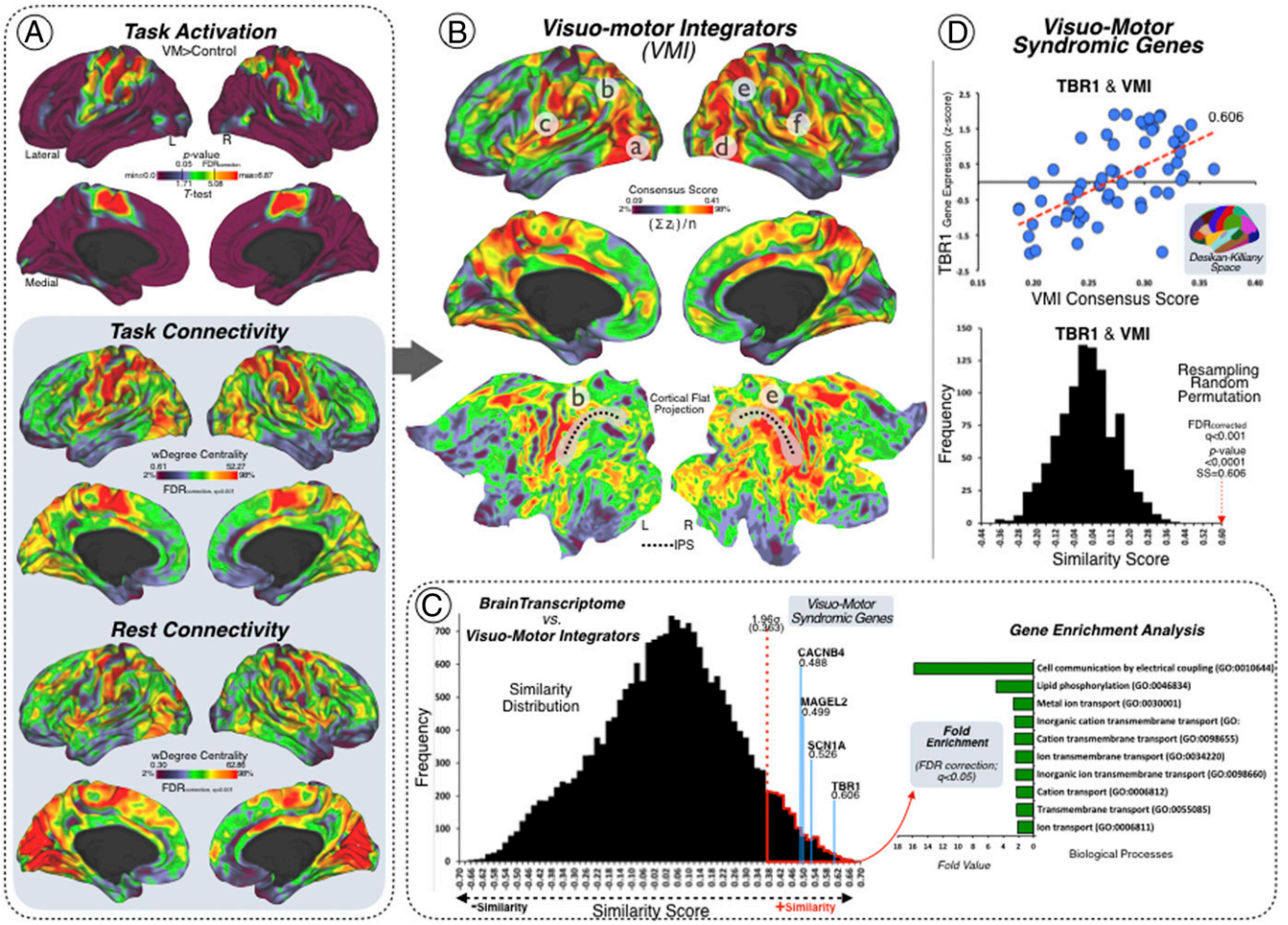

Fig. 1. Neuroimaging–genetics results. (*A*) Three FDR-corrected source brain maps were used for determining the VMI network. (*Top*) The task-functional MRI activation results related to conducting group-level analysis of a finger-tapping task. (*Middle*) The task-functional connectivity results associated with the same finger-tapping task. (*Bottom*) The resting-state functional connectivity results of an independent sample. Each analysis result is displayed in left and right cortical hemispheric surfaces, with lateral and medial projections, and a clear brain color scale (minimum = 2% and maximum = 98% threshold visualization). (*B*) Visuomotor integrators. Left and right cortical hemispheric surfaces of the VMI network map as a result of combining the three source brain maps (from *A*): task activation, task connectivity, and rest connectivity. Letters mark the lateral occipital cortex (a and d), the OP4 (c and f), and the IPS (b, e, and black dotted line). Lateral, medial, and flat projections were used in a clear brain color scale (minimum = 2% and maximum = 98% threshold visualization). (*C*) Syndromic genes linked to the VMI network. (*Left*) The similarity distribution represents the results of the topographical similarity analysis between the VMI network cortical map and the brain transcriptome map (cortical gene expression map of ∼20,000 protein-coding genes). Genes with high cortical expression within the VMI network have high similarity score (red dotted line above 1.96 SDs). (*Right*) Fold enrichment (FE) representation of the GO biological profiles of the genes with high cortical expression within the VMI network (FE >2; statistically significant FDR-corrected $q < 0.05$). (*D*) TBR1 gene and the VMI network. (*Bottom*) Scatter plot showing the topographical similarity relationship between the VMI network map and the cortical gene expression of the TBR1 gene across the Desikan–Killiany atlas (linear fit = red dotted line). (*Top*) Null distribution of the topographical similarity based on a resampling random permutation approach. The red dotted arrow marks the similarity coefficient and the statistically significant *P* value of the topographical similarity relationship between the VMI network map and the cortical gene expression of the TBR1 gene. L, left; R, right; min, minimum; max, maximum; SS, spatial similarity.

motor programming, and the integration of visual and motor information, for example the dorsal and ventral pathways of information processing (46) or the mirror neuron system (47). In accordance with results from the current study, previous research has found strong connectivity between parietal and premotor areas (48–50); also, a multimodal integration network comprising frontal, parietal, and temporoparietal areas has been described (51, 52). Accordingly, we found that brain areas where visual and motor information converge—the lateral occipital, the IPS, and perisylvian regions in the OP and frontal operculum—delineate the VMI network.

Neuroimaging and Genetics of the VMI System. The combination of neuroimaging and genetic information is a promising tool for discovering key biological features of the VMI brain system. Using our consensus map and the AHBA, we were able to identify a set of genes whose cortical expression had highly significant spatial similarity to the VMI network. We observed that this VMI-spatially related gene set exhibited cellular overrepresented functionalities in key domains for cellular and neuronal communicability (e.g., membrane transport, axons of neurons, or GABAergic synapses). Importantly, among all of the genes detected, we found that the cortical expression of four genes from our preselected group of neurogenetic syndromes—TBR1 [ASD (53, 54)], MAGEL2 [Prader–Willi syndrome (53, 54)], and SCN1A and CACNB4 [Dravet syndrome (3, 55–59)]—displayed a high spatial overlap with the VMI map. While the exact implications of these four genes in VMI remain speculative, all of them are known to support molecular functions crucial for optimal development and communication between neurons. For instance, TBR1 expression

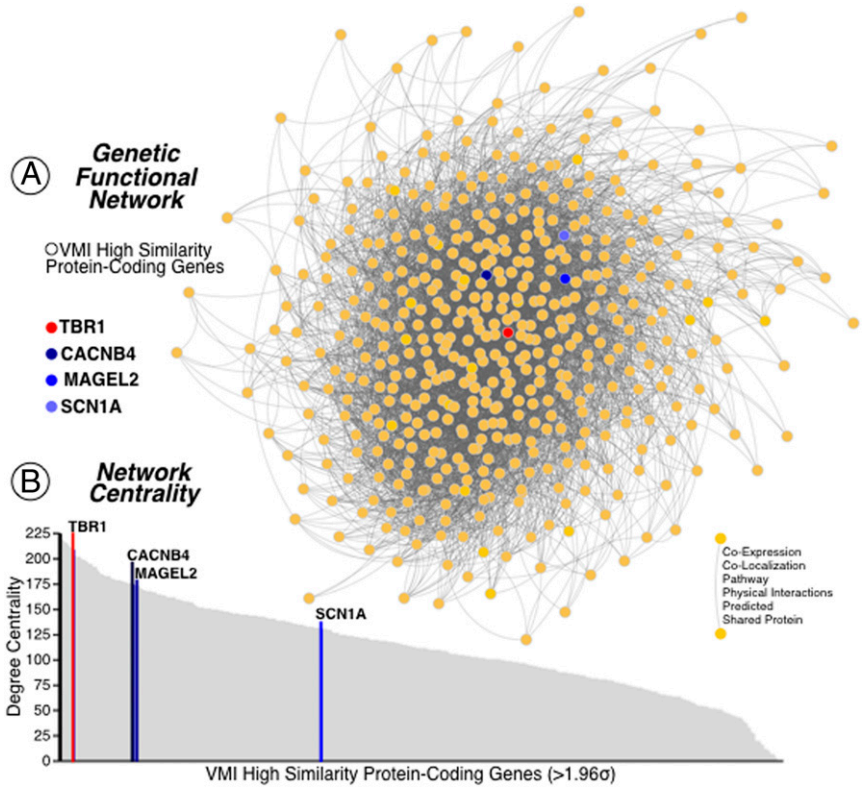

Fig. 2. Genetic network analysis. (*A*) The protein-coding genes from the AHBA with high cortical expression within the VMI network (above 1.96 SDs) are displayed in the network topological space. (*B*) The genes are plotted as a function of the network's degree centrality. The genes related to neurodevelopmental disorders are highlighted in matching colors in *A* and *B*. The TBR1 gene is represented in red and the other three syndromic genes—CACNB4, MAGEL2, and SCN1A—are represented in darker to lighter blue tones.

has been related to the control of neural development in different brain regions (60, 61). Previous studies have uncovered the genetic link between TBR1 and increased risk for ASD (53, 62). At the behavioral level, several studies have found VMI deficits (22, 63, 64) and motor impairment in individuals presenting with ASD (65, 66). It is likely that the high expression of TBR1 in the VMI network may result in neuronal changes impacting its functionality, conferring prototypic behavioral phenotypes in ASD individuals. Moreover, almost one-fifth of patients with Prader–Willi syndrome also present ASD symptoms, and MAGEL2 mutations could be the cause of this comorbidity (54, 67, 68) MAGEL2, which is predominantly expressed in the brain, has been associated with neuronal differentiation and neuronal maintenance (69, 70). Similar to ASD, individuals with Prader–Willi syndrome present VMI difficulties, including impairments in visual perception and motor coordination (5–7, 24, 71, 72). In these patients, VMI abilities decline with age (5, 6). Finally, some associations could be made between the alteration of voltage-gated sodium channels—which can lead to nervous system disorders, such as Dravet syndrome—and SCN1A mutations that cause functional impairments in the intercommunicability of brain neurons through GABAergic connectivity (59, 73–78). Moreover, CACNB4 mutations—also related to Dravet syndrome—are biologically related to calcium channels, which control synaptic transmission at neuronal terminals (55, 58). The combination of SCN1A and CACNB4 mutations may result in particularly aggravated clinical conditions associated with Dravet syndrome (55, 79). During the early stages of Dravet syndrome there is often a disruption of neuronal communicability, which produces early visual and visuomotor dysfunctionality (3). Overall, our findings provide insights about the potential neurobiological bases for common VMI impairments in specific neurogenetic syndromes. We report 485 genes associated with VMI, candidate genes requiring further exploration to investigate potential novel genotypes associated with these and other VMI-related disorders. Future studies with larger sample sizes and/or specific clinical cohorts featuring some of the syndromes studied here (e.g., ASD, Prader–Willi syndrome, or Dravet syndrome) would be ideal in this regard. The methodological approach used here could also be used for studying other phenotypic features in these and other central nervous system syndromes. Further investigation may help close the gap between observed symptoms and biological underpinnings. In future years, high-resolution brain transcriptomic data, like the AHBA, will likely become more widely available. This increased availability would improve our ability to understand how the brain functions across multiple scales, particularly in the interaction between genetic expression and functional network processing.

Conclusions

Our characterization of multimodal interactions (visual and motor cortices) in a specific VMI network facilitates the study of perception-to-action processes and allows the investigation of their underlying neurobiology. We first studied the neuroimaging–genetic relationships across the cortical mantle, following the framework that VMI is shaped by topological overlap between brain activity (goal-directed and spontaneous), connectivity, and genetic interactions. Although additional experimental work is needed to fully understand the relationship between genes of the VMI network system and behavioral impairment, we have described key intersections between the VMI and cortical genes with the help of the AHBA and clinical–genetic knowledge of several neurogenetic syndromes. We showed that our findings regarding TBR1 (ASD), and to a lesser extent MAGEL2 (Prader–Willi), SCN1A (Dravet), and CACNB4 (Dravet), are not only relevant protein-coding genes within the neuronal systems of

VMI but are also likely important in the understanding of VMI impairments and neurocognitive development of the VMI cortical system.

Methods

Participants. We used data from two different cohorts. Cohort 1 consisted of 23 participants (8/15 female/male; mean age = 56.39 y, SD = 8.60; range = 42 to 74) that completed an MRI experiment comprising a high-resolution anatomical scan and a task-activation scan. All participants included in the sample were right-handed (80) and had normal or corrected-to-normal vision. Additionally, all participants were screened for neurological or psychiatric history and reported no past or current drug use. Participants provided written informed consent and all research protocols were approved by the University of Navarra Research Ethics Committee. Cohort 2 consisted of 23 participants (8/15 female/male; mean age = 56.70 y, SD = 9.00; range = 41 to 75) from The Brain Genomics Superstruct Project database (https://www.neuroinfo.org/gsp). Participants in cohort 2 were selected according to their handedness (right-handed), age, and sex to match characteristics of cohort 1. Participants in cohort 2 completed a full MRI and neuropsychological protocol (details available in ref. 81). Only the high-resolution anatomical scan and the resting-state scan were used in the present study.

Functional MRI Task, Data Acquisition, and Image Preprocessing. VMI task, data acquisition, and image preprocessing details are provided in *SI Appendix*.

Image postprocessing.

Task activation analysis. The task activation effects in each voxel were estimated by the general linear model and by modeling the data at the block level (SPM12 Wellcome Department of Imaging Neuroscience, London; https://www.fil.ion.ucl.ac.uk/spm/). The blood oxygenation level-dependent (BOLD) signal was estimated through the convolution of the stimuli with the canonical hemodynamic response function. Six motion realignment parameters were included to explain signal variations due to head motion, that is, as covariates of no interest. From the ordered sequence of movements, the first-level analyses resulted in two contrast images: 1) visual condition and 2) execution condition. In second-level analyses a mean image of the tapping task was obtained after conducting a whole-brain one-sample *t* test analysis. The results were $q < 0.05$ FDR voxel-level-corrected. The corrected task-activation map was normalized using a z-score normalization approach.

SFC analysis. The SFC analysis has been described as a network analysis technique to investigate the integration of information from different brain systems at the functional connectivity level (52). In the present study, SFC analysis was used to describe a functional connectivity pathway that supports the integration of perception–action processes, more specifically the integration of visual and motor connectivity. In-house–developed coding was used for SFC analysis that was run in MATLAB software (MATLAB R2015b; The MathWorks Inc.). Briefly, a mask of 6,185 voxels covering the entire brain was used and SFC analyses were conducted at the individual level to 1) obtain connectivity matrices by calculating Pearson product–moment correlation coefficients (*r* values and their *P* values) for the time course of all brain voxels in a pairwise manner, obtaining the *r* value matrix and the *P* value matrix for each participant and each set of images; 2) retain positive correlations to eliminate deleterious associations between voxels due to interpretational ambiguity (82, 83); and 3) correct each individual's connectivity matrix by controlling for the rate of false positives with an FDR approach (ref. 84; a $q < 0.001$ FDR correction was applied to the *P* values matrix, resulting in only *r* values with corrected *P* values). These final individual association matrices (i.e., corrected *P* value matrices as weighted graphs) were used for the SFC analysis (represented as a simplified brain graph in Fig. 3*B*). For the subsequent SFC analysis, seed regions located in the primary visual cortex (left V1: Montreal Neurological Institute [MNI] −6 −77 11; right V1: MNI 10 −77 9) and primary motor cortex (left M1: MNI: −30 −13 65 and right M1: MNI 34 −13 65) were defined as 3-mm-radius spheres. The coordinates of the seed regions were extracted from previous literature devoted to the study of visual and motor functional pathways (51). This study confirmed that these seed locations are able to detect the modularity of the visual and motor cortices (represented as yellow and green dots in the brain graphs in Fig. 3*B*). A binary mask was created for each seed region, one mask containing the left hemisphere seeds, V1 and M1, and the other mask containing the right hemisphere seeds, V1 and M1. SFC identifies brain regions connected to specified seed regions (i.e., nodes) at different step distances (i.e., links or edges), where the number of steps equals the number of edges needed for connecting one brain voxel to a target node (52). First, at the individual level and in a voxelwise approach, the weighted degree of stepwise connectivity was calculated by summing the weight of edges from a given single brain voxel to both seed regions (left V1–M1 or right V1–M1). The edges included were those with a length of one-link step (i.e., a direct connection) or a length of two-link steps (i.e., an indirect connection) (see the small diagram at the bottom right of Fig. 3*B*).

Direct connectivity for voxel *i* was computed as

$$DC(i) = \sum_s FC(s, i),$$

where *FC* is the FDR thresholded functional connectivity matrix (FDR-corrected) and *s* is each voxel within each seed mask.

Indirect connectivity for voxel *i* was computed as

$$IC(i) = \frac{\sum_s \sum_{j=1}^{n} FC(s,j) * FC(j,i)}{\max(FC * FC)},$$

where *n* is the number of voxels in the brain.

Second, the connectivity degree of all one- and two-link step distances was calculated and set aside as interconnector SFC matrices, which expressed the total number of direct and indirect (at two steps) links from each interconnector node to V1 and M1. The direct interconnector SFC matrix was computed as

$$IDC(i,j) = \sum_s FC(i,s)FC(s,j).$$

The indirect interconnector SFC matrix was computed as

$$IIC(i,j) = \frac{\sum_s \left(\sum_{k=1}^{n} FC(i,k) * FC(k,s) \sum_{l=1}^{n} FC(s,l) * FC(l,j)\right)}{\max(FC * FC)}.$$

Finally, the mean interconnector map was computed using the normalized z-score version, using the following equations:

$$\text{Normalized direct interconnector map } DI(i) = \frac{\left(\sum_{j=1}^{n} IDC(i,j)\right) - m}{s},$$

where $m = \frac{\sum_{i=1}^{n}\sum_{j=1}^{n} IDC(i,j)}{n}$ and $s = \sqrt{\frac{\sum_{i=1}^{n}\left(\sum_{j=1}^{n} IDC(i,j) - m\right)^2}{n}}$.

$$\text{Normalized indirect interconnector map } II(i) = \frac{\left(\sum_{j=1}^{n} IIC(i,j)\right) - m}{s},$$

where $m = \frac{\sum_{i=1}^{n}\sum_{j=1}^{n} IIC(i,j)}{n}$ and $s = \sqrt{\frac{\sum_{i=1}^{n}\left(\sum_{j=1}^{n} IIC(i,j) - m\right)^2}{n}}$.

From this analysis, two interconnector SFC maps were obtained for each dataset (task or resting state): one for left V1–M1 and one for right V1–M1. This analytical strategy determined the nodal interconnectors that link V1 and M1 in the entire cortex in the task and rest connectivity data. A final consensus VMI network map was obtained by calculating the mean map of the normalized task-activation map, task-connectivity SFC map, and rest-connectivity SFC map.

Combination of neuroimaging and AHBA.

Spatial similarity analysis. We used the AHBA to investigate the spatial similarities between protein-coding genetic profiles and our VMI consensus map (Fig. 3 *C* and *D*). The AHBA provides whole-brain genome-wide expression patterns for six human subjects (85). For the spatial similarity strategy, we used the surface anatomical transformation of the transcription profiles, which includes 20,737 protein-coding genes, based on 58,692 measurements of gene expression in 3,702 brain samples obtained from those six adult human subjects (86). The surface anatomical transformation is based on the 68 cortical regions of the Desikan–Killiany atlas (87), which covers the entire cortex and uses individual vectors of the median cortical expression of the genes across the 68 cortical regions (Fig. 3*C*). The spatial similarity analysis was done by means of MATLAB in-house–developed coding (MATLAB R2015b; The MathWorks Inc.). The aim of the spatial similarity analysis was to find which genes, from the 20,737 genes of the AHBA, had a cortical expression that matched the brain regions identified in the VMI network map. We built a null hypothesis distribution by comparing the entire transcriptome with the VMI network map. Then, we detected which genes conferring risk for specific neurogenetic syndromes surpassed a significant spatial correlation value in the upper tail of the null hypothesis distribution (threshold of *r* value >1.96 SDs; red area in Fig. 3*D*). The a priori neurodevelopmental syndromes studied were ASD, Dravet, Fragile X, Prader–Willi, Turner, and Williams. An individual list of the chromosomes impaired in each syndrome along with the genes selected (also called visuomotor syndromic genes throughout the text; $n = 80$) within the chromosomes for this

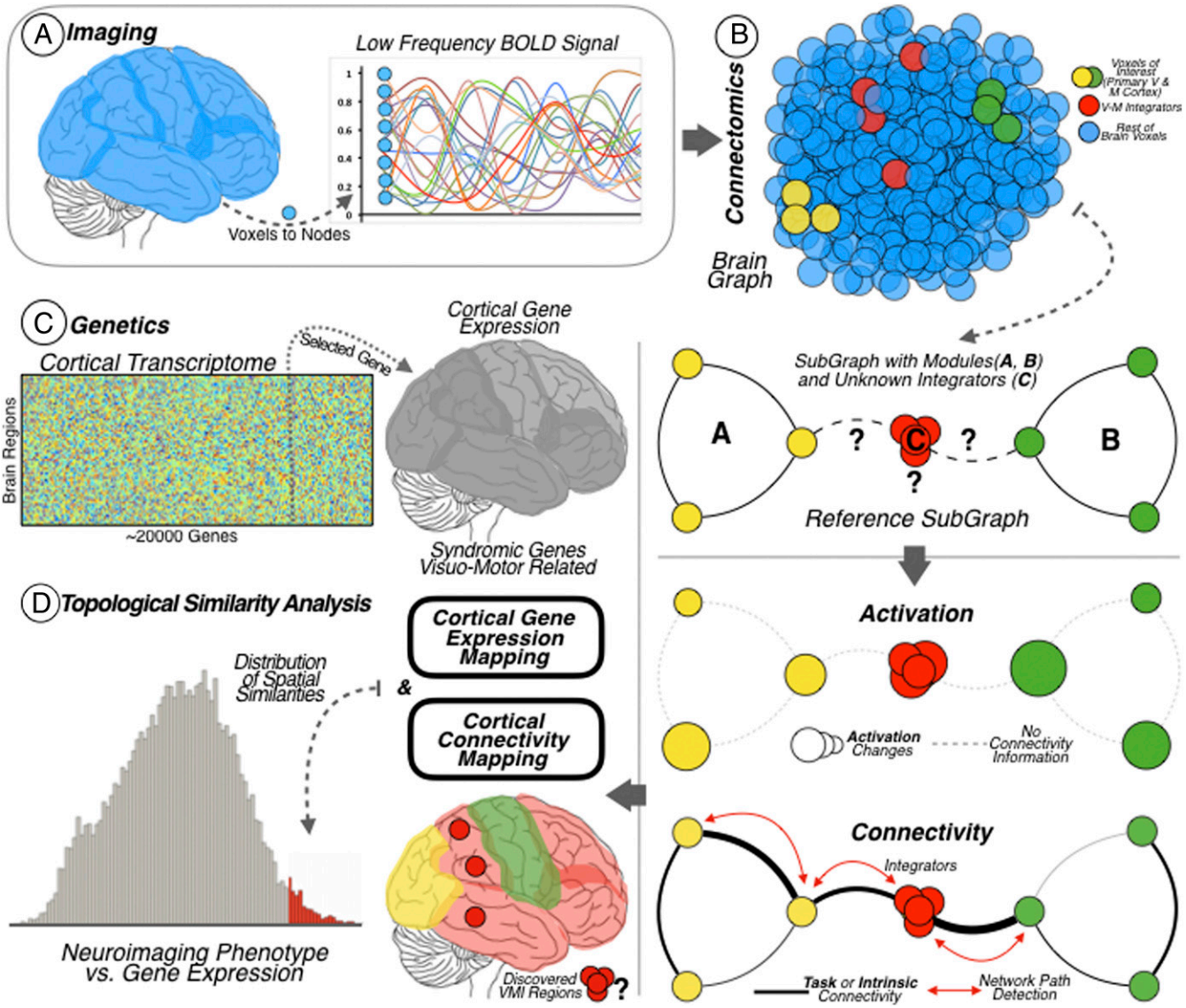

Fig. 3. Pipeline overview. (*A*) Neuroimaging data. Functional MRI BOLD data of the cerebral cortex was recorded at the voxel level for subsequent graph functional connectivity analysis at the node level. (*B*) VMI network. Degree centrality analysis was used to investigate the whole-brain functional connectivity of all brain nodes. Then, SFC was used to investigate the connections departing from modal areas with the aim of discovering their intersection. Two modal areas were studied: the primary visual cortex (represented as yellow dots and as the modal network A) and the primary motor cortex (represented as green dots and as the modal network B). The method revealed the cortical areas supporting the integration of visual and motor information (represented as red dots and as the modal network C). (*Bottom*) Brain functional connectivity graphs derived from resting-state and task datasets were combined with a task-activation dataset for building the VMI network cortical map. Task activation detects the activation changes throughout the cortex and functional connectivity points out the connections (links or paths) between cortical regions. (*C*) Brain genetics. Diagram of the genetic expression matrix for the 20,737 protein-coding genes from the AHBA, across the 68 brain cortical regions included in the surface anatomical transformation of the Desikan–Killiany atlas. The brain map allows investigating whole-brain transcriptome including the genetic expression levels of syndromic genes associated with visuomotor functions. (*D*) Neuroimaging–genetics relation. A topographical similarity analysis was done between the VMI network cortical map and the cortical gene expression map of the syndromic genes. This analysis allows localizing the genes with high cortical expression within the VMI network map (area of the histogram highlighted in red, corresponds to similarity scores above 1.96 SDs).

study was based on GeneReviews (https://www.ncbi.nlm.nih.gov/books/NBK1116 as of June 2018; *SI Appendix*, Table S1). Next, we used a resampling strategy to calculate the corrected *P* value of each similarity comparison between specific genes and the VMI network map. We used MATLAB's random permutation function and 1,000 iterations to probe if solid topological associations exist between targeted genes and the VMI map. The random permutation analysis was calculated over 1) each gene's median cortical expression extracted from the AHBA across the 68 cortical regions included in the surface anatomical transformation based on the Desikan–Killiany atlas and 2) the VMI network map data. Then, for each run of the resampling analysis, the Pearson product–moment correlation coefficient was calculated between the abovementioned variables. Finally, a probability distribution with the results of the resampling analysis was computed for each gene. The statistical significance of spatial VMI and genetic similarity score of each individual gene was corrected using a FDR approach (84); a q <0.001 FDR correction was applied to the *P* values matrix (Fig. 1 and *SI Appendix*, Fig. S1). As a complementary strategy, we tested whether the probability of our correlation values obtained between the genes and the consensus map were due to chance. We generated 1,000 random maps based on the same spatial smoothing level as the one in the consensus map. Then, we obtained the null hypothesis distribution of similarity scores with these random maps and corrected all *P* values with an FDR approach (*SI Appendix*, Fig. S2).

Biological processes of genes mediating visuomotor integration. The list of genes whose spatial cortical expression demonstrated high spatial correlation with the VMI network was entered in a GO term enrichment analysis tool (http://geneontology.org; ref. 88). GO is a genetic annotation resource

dedicated to investigating gene functionalities. In the present research, we used the annotation systems of biological processes and cellular components within GO to characterize our findings. Biological processes are focused on "biological programs accomplished by multiple molecular activities" (88), that is, gene actions that lead to specific objectives, which are done under regulated procedures and temporal sequences. Cellular components are focused on "the locations relative to cellular structures in which a gene product performs a function" (88). We computed PANTHER Overrepresentation Test (21) within the term enrichment analysis tool of the GO resource using the list of genes whose spatial cortical expression demonstrated high spatial correlation with the VMI network. The PANTHER resource classifies protein sequences of genes in terms of their evolutionary history and function, making it possible to formulate inferences about these gene functions (a detailed description of PANTHER is available in ref. 21). During the PANTHER Overrepresentation Test, the *Homo sapiens* list (with all of the genes included in the database) was selected as the reference list and the GO biological processes and cellular components were selected as the annotation datasets. A binomial test was then conducted ($P < 0.05$ FDR-corrected) for each annotation data set. The results of the analysis were based on their relative term enrichment, which represents to what extent each annotation is statistically represented in a set of given genes.

Interactome analysis. Using an interactome approach, we validated our genetic findings beyond their spatial colocalizations with the VMI cortical map. We used Genemania (http://genemania.org/ and ref. 89) and Cytoscape (https://cytoscape.org/ and ref. 90) software to perform an interactome analysis and degree centrality assessment of the set of genes obtained in the spatial similarity analysis. We used Genemania's composite gene–gene interaction profile from coexpressions, colocalizations, genetic interactions, pathways, predicted physical interactions, and shared protein domains (89).

Materials, Data, and Code Availability.

Neuroimaging data. The neuroimaging dataset acquired during the task-MRI paradigm is available from the corresponding author upon request and the dataset acquired during the resting-state MRI paradigm from the Human Connectome Project website (http://www.humanconnectomeproject.org).

Genetic data. The genetic data that support the findings of this study are available from the AHBA website (https://human.brain-map.org).

Code availability. All codes for imaging analysis are available for the research community from the corresponding author upon request.

ACKNOWLEDGMENTS. This research was supported by grants from the National Institutes of Health (K23EB019023, R01AG061811, and R01AG061445 to J.S.). E.B. was funded by a research stay grant from the Spanish Government (2017 José Castillejo for young Ph.D. researchers) and a postdoctoral research grant from the Generalitat Valenciana and the European Social Fund ("Investing in your future"; 2018 APOSTD).

1. C. Dravet, H. Oguni, "Dravet syndrome (severe myoclonic epilepsy in infancy)" in *Handbook of Clinical Neurology*, O. Dulac, M. Lassonde, H. B. Sarnat, Eds. (Elsevier, 2013), pp. 627–633.
2. D. Chieffo *et al*., Neuropsychological development in children with Dravet syndrome. *Epilepsy Res.* **95**, 86–93 (2011).
3. M. Wolff, C. Cassé-Perrot, C. Dravet, Severe myoclonic epilepsy of infants (Dravet syndrome): Natural history and neuropsychological findings. *Epilepsia* **47** (suppl. 2), 45–48 (2006).
4. M. Borodyanskaya, S. Coffey, M. Y. Ono, R. J. Hagerman, "Intergenerational effects of mutations in the fragile X mental retardation 1 gene. Fragile X: A model of X-linked mental retardation and neurodegeneration" in *Genes, Brain, and Development*, M. A. Barnes, Ed. (Cambridge University Press, 2010), pp. 3–18.
5. J. Whittington, A. Holland, Cognition in people with Prader-Willi syndrome: Insights into genetic influences on cognitive and social development. *Neurosci. Biobehav. Rev.* **72**, 153–167 (2017).
6. S. T. Lo, P. J. L. Collin, A. C. S. Hokken-Koelega, Visual-motor integration in children with Prader-Willi syndrome. *J. Intellect. Disabil. Res.* **59**, 827–834 (2015).
7. L. Reus, L. A. van Vlimmeren, J. B. Staal, B. J. Otten, M. W. G. Nijhuis-van der Sanden, The effect of growth hormone treatment or physical training on motor performance in Prader-Willi syndrome: A systematic review. *Neurosci. Biobehav. Rev.* **36**, 1817–1838 (2012).
8. J. Rovet, Turner syndrome: A review of genetic and hormonal influences on neuropsychological functioning. *Child Neuropsychol.* **10**, 262–279 (2004).
9. M. W. G. Nijhuis-van der Sanden, P. A. T. M. Eling, B. J. Otten, A review of neuropsychological and motor studies in Turner syndrome. *Neurosci. Biobehav. Rev.* **27**, 329–338 (2003).
10. L. J. Lewandowski, Clinical syndromes among the learning disabled. *J. Learn. Disabil.* **18**, 177–178 (1985).
11. J. Atkinson, The davida teller award lecture, 2016: Visual brain development: A review of "dorsal stream vulnerability"-motion, mathematics, amblyopia, actions, and attention. *J. Vis.* **17**, 26 (2017).
12. C. A. Morris, "Williams Syndrome" in *GeneReviews*, M. P. Adam *et al*., Eds. (University of Washington, Seattle, WA, 2017).
13. M. Miller, L. Chukoskie, M. Zinni, J. Townsend, D. Trauner, Dyspraxia, motor function and visual-motor integration in autism. *Behav. Brain Res.* **269**, 95–102 (2014).
14. K. A. Fournier, C. J. Hass, S. K. Naik, N. Lodha, J. H. Cauraugh, Motor coordination in autism spectrum disorders: A synthesis and meta-analysis. *J. Autism Dev. Disord.* **40**, 1227–1240 (2010).
15. H. Memisevic, M. Djordjevic, Visual-motor integration in children with mild intellectual disability: A meta-analysis. *Percept. Mot. Skills* **125**, 696–717 (2018).
16. K. E. Beery, N. A. Beery, "Beery VMI: The Beery-Buktenica developmental test of visual-motor integration with supplemental developmental tests of visual perception and motor coordination and stepping stones age norms from birth to age six" in *Administration, Scoring, and Teaching Manual* (PsychCorp, New York, 2010).
17. B. Wiśniowiecka-Kowalnik, B. A. Nowakowska, Genetics and epigenetics of autism spectrum disorder-current evidence in the field. *J. Appl. Genet.* **60**, 37–47 (2019).
18. T. N. Turner *et al*., Genome sequencing of autism-affected families reveals disruption of putative noncoding regulatory DNA. *Am. J. Hum. Genet.* **98**, 58–74 (2016).
19. E. M. Dykens, E. Lee, E. Roof, Prader-Willi syndrome and autism spectrum disorders: An evolving story. *J. Neurodev. Disord.* **3**, 225–237 (2011).
20. E. H. Shen, C. C. Overly, A. R. Jones, The Allen Human Brain Atlas: Comprehensive gene expression mapping of the human brain. *Trends Neurosci.* **35**, 711–714 (2012).
21. H. Mi *et al*., PANTHER version 11: Expanded annotation data from gene ontology and reactome pathways, and data analysis tool enhancements. *Nucleic Acids Res.* **45**, D183–D189 (2017).
22. R. R. Green *et al*., Beery VMI performance in autism spectrum disorder. *Child Neuropsychol.* **22**, 795–817 (2016).
23. C. Cassé-Perrot, M. Wolff, C. Dravet, "Neuropsychological aspects of severe myoclonic epilepsy in infancy" in *Neuropsychology of Childhood Epilepsy. Advances in Behavioral Biology*, I. Jambaqué, M. Lassonde, O. Dulac, Eds. (Springer, 2001), vol. 50, pp. 131–140.
24. R. T. Schultz *et al*., Visual-motor integration functioning in children with Tourette syndrome. *Neuropsychology* **12**, 134–145 (1998).
25. A. Herwig, Linking perception and action by structure or process? Toward an integrative perspective. *Neurosci. Biobehav. Rev.* **52**, 105–116 (2015).
26. G. Erdogan, Q. Chen, F. E. Garcea, B. Z. Mahon, R. A. Jacobs, Multisensory part-based representations of objects in human lateral occipital cortex. *J. Cogn. Neurosci.* **28**, 869–881 (2016).
27. M. J. Naumer *et al*., Visuohaptic convergence in a corticocerebellar network. *Eur. J. Neurosci.* **31**, 1730–1736 (2010).
28. T. W. James *et al*., Haptic study of three-dimensional objects activates extrastriate visual areas. *Neuropsychologia* **40**, 1706–1714 (2002).
29. A. Amedi, R. Malach, T. Hendler, S. Peled, E. Zohary, Visuo-haptic object-related activation in the ventral visual pathway. *Nat. Neurosci.* **4**, 324–330 (2001).
30. U. Halsband, R. K. Lange, Motor learning in man: A review of functional and clinical studies. *J. Physiol. Paris* **99**, 414–424 (2006).
31. G. Rizzolatti, D. M. Wolpert, Motor systems. *Curr. Opin. Neurobiol.* **15**, 623–625 (2005).
32. G. Gentile, V. I. Petkova, H. H. Ehrsson, Integration of visual and tactile signals from the hand in the human brain: An fMRI study. *J. Neurophysiol.* **105**, 910–922 (2011).
33. E. Wacker, B. Spitzer, R. Lützkendorf, J. Bernarding, F. Blankenburg, Tactile motion and pattern processing assessed with high-field fMRI. *PLoS One* **6**, e24860 (2011).
34. S. B. Eickhoff *et al*., Anatomical and functional connectivity of cytoarchitectonic areas within the human parietal operculum. *J. Neurosci.* **30**, 6409–6421 (2010).
35. J. P. Young *et al*., Somatotopy and attentional modulation of the human parietal and opercular regions. *J. Neurosci.* **24**, 5391–5399 (2004).
36. S. Vahdat, M. Darainy, T. E. Milner, D. J. Ostry, Functionally specific changes in resting-state sensorimotor networks after motor learning. *J. Neurosci.* **31**, 16907–16915 (2011).
37. B. Pleger *et al*., Pharmacological suppression of plastic changes in human primary somatosensory cortex after motor learning. *Exp. Brain Res.* **148**, 525–532 (2003).
38. G. J. Zelinsky, J. W. Bisley, The what, where, and why of priority maps and their interactions with visual working memory. *Ann. N. Y. Acad. Sci.* **1339**, 154–164 (2015).
39. F. Katsuki, C. Constantinidis, Bottom-up and top-down attention: Different processes and overlapping neural systems. *Neuroscientist* **20**, 509–521 (2014).
40. R. J. Krauzlis, L. P. Lovejoy, A. Zénon, Superior colliculus and visual spatial attention. *Annu. Rev. Neurosci.* **36**, 165–182 (2013).
41. J. W. Bisley, M. E. Goldberg, Attention, intention, and priority in the parietal lobe. *Annu. Rev. Neurosci.* **33**, 1–21 (2010).
42. J. T. Serences, S. Yantis, Selective visual attention and perceptual coherence. *Trends Cogn. Sci.* **10**, 38–45 (2006).
43. G. Deco, E. T. Rolls, A neurodynamical cortical model of visual attention and invariant object recognition. *Vision Res.* **44**, 621–642 (2004).
44. J. C. Culham, K. F. Valyear, Human parietal cortex in action. *Curr. Opin. Neurobiol.* **16**, 205–212 (2006).
45. R. M. de Azevedo Neto, E. Amaro Júnior, Bilateral dorsal fronto-parietal areas are associated with integration of visual motion information and timed motor action. *Behav. Brain Res.* **337**, 91–98 (2018).
46. L. Ungerleider, M. Mishkin, "Two cortical visual systems" in *The Analysis of Visual Behaviour*, D. Ingle, M. A. Goodale, R. J. W. Mansfield, Eds. (MIT Press, 1982), pp. 549–586.

47. G. Rizzolatti, L. Craighero, The mirror-neuron system. *Annu. Rev. Neurosci.* **27**, 169–192 (2004).
48. A. Battaglia-Mayer, R. Caminiti, "Parieto-frontal networks for eye–hand coordination and movements" in *Handbook of Clinical Neurology*, G. Vallar, H. Branch Colsett, Ed. (Elsevier, 2018), vol. 151, pp. 499–524.
49. G. Rizzolatti, S. Rozzi, "The mirror mechanism in the parietal lobe" in *Handbook of Clinical Neurology*, G. Vallar, H. Branch Colsett, Eds. (Elsevier, 2018), vol. 151, pp. 499–524.
50. G. Rizzolatti, C. Sinigaglia, The functional role of the parieto-frontal mirror circuit: Interpretations and misinterpretations. *Nat. Rev. Neurosci.* **11**, 264–274 (2010).
51. J. Sepulcre, Functional streams and cortical integration in the human brain. *Neuroscientist* **20**, 499–508 (2014).
52. J. Sepulcre, M. R. Sabuncu, T. B. Yeo, H. Liu, K. A. Johnson, Stepwise connectivity of the modal cortex reveals the multimodal organization of the human brain. *J. Neurosci.* **32**, 10649–10661 (2012).
53. H. C. Chuang, T. N. Huang, Y. P. Hsueh, T-Brain-1–A potential master regulator in autism spectrum disorders. *Autism Res.* **8**, 412–426 (2015).
54. C. P. Schaaf *et al*., Truncating mutations of MAGEL2 cause Prader-Willi phenotypes and autism. *Nat. Genet.* **45**, 1405–1408 (2013).
55. I. Ohmori *et al*., CACNA1A variants may modify the epileptic phenotype of Dravet syndrome. *Neurobiol. Dis.* **50**, 209–217 (2013).
56. C. Dravet, The core Dravet syndrome phenotype. *Epilepsia* **52** (suppl. 2), 3–9 (2011).
57. F. Guzzetta, Cognitive and behavioral characteristics of children with Dravet syndrome: An overview. *Epilepsia* **52** (suppl. 2), 35–38 (2011).
58. I. Ohmori *et al*., A CACNB4 mutation shows that altered Ca(v)2.1 function may be a genetic modifier of severe myoclonic epilepsy in infancy. *Neurobiol. Dis.* **32**, 349–354 (2008).
59. L. Claes *et al*., De novo mutations in the sodium-channel gene SCN1A cause severe myoclonic epilepsy of infancy. *Am. J. Hum. Genet.* **68**, 1327–1332 (2001).
60. A. B. Mihalas, R. F. Hevner, Control of neuronal development by T-box genes in the brain. *Curr. Top. Dev. Biol.* **122**, 279–312 (2017).
61. F. Bedogni *et al*., Autism susceptibility candidate 2 (Auts2) encodes a nuclear protein expressed in developing brain regions implicated in autism neuropathology. *Gene Expr. Patterns* **10**, 9–15 (2010).
62. B. J. O'Roak *et al*., Multiplex targeted sequencing identifies recurrently mutated genes in autism spectrum disorders. *Science* **338**, 1619–1622 (2012).
63. S. D. Mayes, S. L. Calhoun, Learning, attention, writing, and processing speed in typical children and children with ADHD, autism, anxiety, depression, and oppositional-defiant disorder. *Child Neuropsychol.* **13**, 469–493 (2007).
64. S. C. Fulkerson, W. M. Freeman, Perceptual-motor deficiency in autistic children. *Percept. Mot. Skills* **50**, 331–336 (1980).
65. R. Khalil, R. Tindle, T. Boraud, A. A. Moustafa, A. A. Karim, Social decision making in autism: On the impact of mirror neurons, motor control, and imitative behaviors. *CNS Neurosci. Ther.* **24**, 669–676 (2018).
66. R. L. Moseley, F. Pulvermüller, What can autism teach us about the role of sensorimotor systems in higher cognition? New clues from studies on language, action semantics, and abstract emotional concept processing. *Cortex* **100**, 149–190 (2018).
67. M.-J. Descheemaeker, V. Govers, P. Vermeulen, J.-P. Fryns, Pervasive developmental disorders in Prader-Willi syndrome: The leuven experience in 59 subjects and controls. *Am. J. Med. Genet. A.* **140**, 1136–1142 (2006).
68. I. Boccaccio *et al*., The human MAGEL2 gene and its mouse homologue are paternally expressed and mapped to the Prader-Willi region. *Hum. Mol. Genet.* **8**, 2497–2505 (1999).
69. S. Bervini, H. Herzog, Mouse models of Prader-Willi syndrome: A systematic review. *Front. Neuroendocrinol.* **34**, 107–119 (2013).
70. S. Lee *et al*., Expression and imprinting of MAGEL2 suggest a role in Prader-willi syndrome and the homologous murine imprinting phenotype. *Hum. Mol. Genet.* **9**, 1813–1819 (2000).
71. J. Whittington, A. Holland, T. Webb, Relationship between the IQ of people with Prader-Willi syndrome and that of their siblings: Evidence for imprinted gene effects. *J. Intellect. Disabil. Res.* **53**, 411–418 (2009).
72. J. Jauregi *et al*., A neuropsychological assessment of frontal cognitive functions in Prader-Willi syndrome. *J. Intellect. Disabil. Res.* **51**, 350–365 (2007).
73. A. Brunklaus, R. Ellis, E. Reavey, C. Semsarian, S. M. Zuberi, Genotype phenotype associations across the voltage-gated sodium channel family. *J. Med. Genet.* **51**, 650–658 (2014).
74. M. Oliva, S. F. Berkovic, S. Petrou, Sodium channels and the neurobiology of epilepsy. *Epilepsia* **53**, 1849–1859 (2012).
75. C. Marini *et al*., The genetics of Dravet syndrome. *Epilepsia* **52** (suppl. 2), 24–29 (2011).
76. A. Gambardella, C. Marini, Clinical spectrum of SCN1A mutations. *Epilepsia* **50** (suppl. 5), 20–23 (2009).
77. C. E. Stafstrom, Severe epilepsy syndromes of early childhood: The link between genetics and pathophysiology with a focus on SCN1A mutations. *J. Child Neurol.* **24** (suppl. 8), 15S–23S (2009).
78. A. Escayg *et al*., Mutations of SCN1A, encoding a neuronal sodium channel, in two families with GEFS+2. *Nat. Genet.* **24**, 343–345 (2000).
79. A. Escayg, A. L. Goldin, Sodium channel SCN1A and epilepsy: Mutations and mechanisms. *Epilepsia* **51**, 1650–1658 (2010).
80. R. C. Oldfield, The assessment and analysis of handedness: The Edinburgh inventory. *Neuropsychologia* **9**, 97–113 (1971).
81. A. J. Holmes *et al*., Brain Genomics Superstruct Project initial data release with structural, functional, and behavioral measures. *Sci. Data* **2**, 150031 (2015).
82. K. Murphy, R. M. Birn, D. A. Handwerker, T. B. Jones, P. A. Bandettini, The impact of global signal regression on resting state correlations: Are anti-correlated networks introduced? *Neuroimage* **44**, 893–905 (2009).
83. K. R. A. Van Dijk, M. R. Sabuncu, R. L. Buckner, The influence of head motion on intrinsic functional connectivity MRI. *Neuroimage* **59**, 431–438 (2012).
84. Y. Benjamini, D. Drai, G. Elmer, N. Kafkafi, I. Golani, Controlling the false discovery rate in behavior genetics research. *Behav. Brain Res.* **125**, 279–284 (2001).
85. M. J. Hawrylycz *et al*., An anatomically comprehensive atlas of the adult human brain transcriptome. *Nature* **489**, 391–399 (2012).
86. L. French, T. Paus, FreeSurfer view of the cortical transcriptome generated from the Allen Human Brain Atlas. *Front. Neurosci.* **9**, 323 (2015).
87. R. S. Desikan *et al*., An automated labeling system for subdividing the human cerebral cortex on MRI scans into gyral based regions of interest. *Neuroimage* **31**, 968–980 (2006).
88. The Gene Ontology Consortium, Expansion of the Gene Ontology knowledgebase and resources. *Nucleic Acids Res.* **45**, D331–D338 (2017).
89. S. Mostafavi, D. Ray, D. Warde-Farley, C. Grouios, Q. Morris, GeneMANIA: A real-time multiple association network integration algorithm for predicting gene function. *Genome Biol.* **9** (suppl. 1), S4 (2008).
90. C. T. Lopes *et al*., Cytoscape web: An interactive web-based network browser. *Bioinformatics* **26**, 2347–2348 (2010).